Scene-based nonuniformity correction algorithm based on interframe registration

Article *in* Journal of the Optical Society of America A · June 2011

DOI: 10.1364/JOSAA.28.001164 · Source: PubMed

4 authors, including:

Chao Zuo
Nanjing University of Science and Technology
530 PUBLICATIONS **13,611** CITATIONS

SEE PROFILE

Xiubao Sui
Nanjing University of Science and Technology
126 PUBLICATIONS **1,853** CITATIONS

SEE PROFILE

Scene-based nonuniformity correction algorithm based on interframe registration

Chao Zuo,* Qian Chen, Guohua Gu, and Xiubao Sui

National Defense Key Laboratory of Optoelectronic Engineering, Nanjing University of Science and Technology, Nanjing, Jiangsu Province 210094, China
**Corresponding author: surpasszuo@163.com*

Received January 4, 2011; revised February 26, 2011; accepted February 26, 2011; posted March 10, 2011 (Doc. ID 140108); published May 20, 2011

In this paper, we present a simple and effective scene-based nonuniformity correction (NUC) method for infrared focal plane arrays based on interframe registration. This method estimates the global translation between two adjacent frames and minimizes the mean square error between the two properly registered images to make any two detectors with the same scene produce the same output value. In this way, the accumulation of the registration error can be avoided and the NUC can be achieved. The advantages of the proposed algorithm lie in its low computational complexity and storage requirements and ability to capture temporal drifts in the nonuniformity parameters. The performance of the proposed technique is thoroughly studied with infrared image sequences with simulated nonuniformity and infrared imagery with real nonuniformity. It shows a significantly fast and reliable fixed-pattern noise reduction and obtains an effective frame-by-frame adaptive estimation of each detector's gain and offset.

OCIS codes: 040.1240, 100.2000, 100.2550, 100.2980, 110.3080.

1. INTRODUCTION

Infrared focal plane array (IRFPA) sensors are widely used in the fields of aviation, industry, agriculture, medicine, and scientific research. However, the nonuniformity, produced by mismatches during the fabrication process of the IRFPA can considerably degrade the spatial resolution and temperature resolvability, since it results in a fixed pattern noise (FPN) that is superimposed on the observed images [1,2]. Corresponding nonuniformity correction (NUC) algorithms have been proposed to solve the problem.

NUC techniques are mainly classified into two categories [2], one of which is the calibration-based NUC method. It applies a rather simple theory, and is easy to implement and integrate with hardware. Two-point correction is the most commonly used technique to counteract FPN. It employs two blackbodies at different temperatures to calculate the exact gain and offset of each detector on the IRFPA through the use of a simple line fitting procedure [3–5]. However, the nonuniformity is always influenced by such external conditions as ambient temperature, variation in the transistor bias voltage, and the time-dependent nature of the object irradiance. All these factors have made each detector of the focal plane drift slowly with the time lapse [6]. Therefore, these calibration-based NUC methods require the procedure to be periodically performed so as to guarantee the correction of the temporal drift of the FPN. To make up for the inconvenience, many scene-based NUC (SBNUC) techniques [7–18] have been proposed that, to some degree, overcome the correction error caused by the drifting response of the IRFPA. The correction coefficients can be adaptively updated according to the scene information.

On the whole, scene-based algorithms are generally identified by two main approaches, namely, statistical methods and registration-based methods. Algorithms based on statistics usually make some spatiotemporal assumptions on the irradiance collected by each detector in the array. Based on these assumptions, some quantities are extracted to estimate the correction coefficients for the FPN. Some representatives of this kind are the temporal high-pass filter technique [7], the constant statistics method [8], neural-network-based NUC [9], and the constant range method and its corresponding extensions [10–12]. The other kind of SBNUC is based on registration. These techniques all use the idea that each detector should have an identical response when observing the same scene point over time. Therefore, registration-based methods require accurate estimation of the motion between frames. Some representatives of this sort of algorithm are O'Neil's method [13], motion compensated average (MCA) [14], and algebraic scene-based algorithms [15].

Statistics-based SBNUC methods are used and studied widely because of their relatively lower computational complexity, smaller storage demands, and better real-time performance. However, they are motion dependent and sensitive to extreme scene [16,17]. Therefore, it is hard to guarantee both the convergence speed and stability of the algorithm. If high convergence speed is pursued excessively, ghosting artifacts are easily generated, superimposing on the new "corrected" scene [17,18]. On the other hand, registration-based NUC algorithms offer higher convergence speed, and almost no ghosting artifacts can be found. However, they are not that practical because of their high computational complexity and large storage demands. Meanwhile, the registration and correction errors can be conveyed accumulatively, seriously affecting the correction accuracy.

This paper puts forward a novel SBNUC algorithm called interframe registration-based least mean square (IRLMS) NUC. In this algorithm, the irradiation of objects is assumed unchanged during the interframe time interval and a

phase-correlation method is adopted for accurate motion estimation. Thus, NUC can be achieved by minimizing the mean square error between two properly aligned images using the least mean square (LMS) algorithm. This paper is organized as follows. In Section 2, a detailed analysis of the correction algorithm put forward by this paper is given. In Section 3, comparisons with two related NUC techniques are presented. The accuracy of the adopted registration method and some performance issues are discussed in Section 4. Experimental results are presented in Section 5. Finally, the conclusions of the paper are summarized in Section 6.

2. NONUNIFORMITY CORRECTION

A. Nonuniformity Observation Model

First, we assume that the photoresponses of the individual detectors in a focal plane array can be characterized by a linear irradiance–voltage model [19], and their output is given by

$$Y_n(i,j) = g_n(i,j) \cdot X_n(i,j) + o_n(i,j). \tag{1}$$

Here, subscript n is the frame index. $g_n(i,j)$ and $o_n(i,j)$ are, respectively, the real gain and offset of the (i,j)th detector. $X_n(i,j)$ stands for the real incident infrared photon flux collected by the respective detector, and the observed pixel value is given by $Y_n(i,j)$. We assume that the gains and offsets drift slowly in time, so they share the same subscript n.

NUC is performed by applying a linear mapping to the observed pixel values $Y_n(i,j)$ to provide an estimate of the true scene value $X_n(i,j)$ so that the detectors appear to be performing uniformly. This correction is given by

$$X_n(i,j) = w_n(i,j) \cdot Y_n(i,j) + b_n(i,j), \tag{2}$$

where $w_n(i,j)$ and $b_n(i,j)$ are, respectively, the gain and offset of the linear correction model of the (i,j)th detector. Their relation with the real gain and offset can be represented by

$$w_n(i,j) = \frac{1}{g_n(i,j)}, \tag{3}$$

$$b_n(i,j) = -\frac{o_n(i,j)}{g_n(i,j)}. \tag{4}$$

Therefore, if ideal estimates of $w_n(i,j)$ and $b_n(i,j)$ or $g_n(i,j)$ and $o_n(i,j)$ can be obtained, then NUC can be realized through Eq. (2).

B. Motion Estimation

Take two images $f_1(x,y)$ and $f_2(x,y)$ into consideration, if there exist relative shifts of x_0 and y_0, respectively, in the horizontal and vertical directions between $f_1(x,y)$ and $f_2(x,y)$, i.e.,

$$f_2(x,y) = f_1(x - x_0, y - y_0). \tag{5}$$

Based on the Fourier shift theorem, their relative translation can be obtained by calculating their normalized cross-power spectrum:

$$\hat{c}(u,v) = \frac{F_2(u,v)F_1^*(u,v)}{|F_2(u,v)F_1^*(u,v)|} = e^{-2\pi j(ux_0+vy_0)}, \tag{6}$$

where the asterisk denotes complex conjugation, $F_1(u,v)$ and $F_2(u,v)$ are, respectively, the Fourier transforms of $f_1(x,y)$ and $f_2(x,y)$, and (u,v) are the Fourier domain coordinates. Once computed, the approach cited in the literature [20] is to compute the inverse Fourier transform of $\hat{c}(u,v)$ and a Dirac delta function can be recognized as an intensity peak. The coordinate of this peak corresponds directly to the translation vector (x_0, y_0).

If the translation of a subpixel is taken into consideration, interpolation by zero padding the cross-power spectrum to a larger array of dimensions $(\kappa M, \kappa N)$ is suggested in [21], where M and N are the image dimensions. Through this method, an estimated translation with κ^{-1} pixel accuracy can be obtained.

In general, when the sensor is at work, the interframe changes of the scene in the field of view are relatively small. The translation between two adjacent observed frames can be obtained by

$$(d_i, d_j) = \underset{i,j}{\operatorname{argmax}} \operatorname{Re}\left\{ \mathrm{FFT}^{-1}\left(\frac{\bar{Y}_n(u,v) \cdot \bar{Y}_{n-1}^*(u,v)}{|\bar{Y}_n(u,v) \cdot \bar{Y}_{n-1}^*(u,v)|} \right) \right\}, \tag{7}$$

where the bar notation indicates the Fourier transform. The changes of the irradiance mainly have an influence on amplitude, with only a minor effect on phase in the frequency domain. Therefore the phase-correlation method is resilient to noise, bad pixels, and other defects typical of infrared images. In this paper, the motion is assumed to consist only of translation, neglecting any scaling, rotation or other warping of the images.

The change of scene irradiation and local motion can be ignored because of the rather short time; if there is no nonuniformity and registration error, then there is obviously

$$Y_n(i,j) = Y_{n-1}(i - d_i, j - d_j) = \mathrm{FFT}^{-1}(\bar{Y}_{n-1}(u,v)e^{-2\pi j(ud_i+vd_j)}). \tag{8}$$

Equation (8) assumes that there is a one-to-one mapping of pixels in the two adjacent frames. This is, of course not true. Some new scene data has inevitably been introduced at the edges of the image, while some has been translated out of the image frame and lost. Evidently, the validity of the equation is confined to the overlapped area between frame $n-1$ and frame n (see Fig. 1).

C. Nonuniformity Correction

From the discussion above, if there is an ideal situation, i.e., registration error can be ignored, and there is no nonuniformity or irradiation change of the scene between the two frames, then the Eq. (8) is established. However, Eq. (8) is never valid due to the presence of random noise and nonuniformity. Therefore, we define the error function:

$$e_n(i,j) = \hat{X}_{n-1}(i - d_i, j - d_j) - \hat{X}_n(i,j). \tag{9}$$

Here the error function $e_n(i,j)$ is defined as the corresponding difference between the two adjacent corrected frames. By contrast, in Scribner's method, the desired image is a blurred version of the observed frame [9]. In our algorithm, the corrected (using estimated parameters) $n-1$th frame is considered to be the reference frame and the shift of the

$$w_{n+1}(i,j) = \begin{cases} w_n(i,j) + a \cdot e_n(i,j) \cdot Y_n(i,j) & \text{when pixel } (i,j) \text{is in the overlapped area} \\ w_n(i,j) & \text{other} \end{cases}, \tag{14}$$

$$b_{n+1}(i,j) = \begin{cases} b_n(i,j) + a \cdot e_n(i,j) & \text{when pixel}(i,j) \text{is in the overlapped area} \\ b_n(i,j) & \text{other} \end{cases}, \tag{15}$$

nth frame is determined with respect to the reference frame. We set the corresponding value in frame $n-1$ as the "target value" of the (i,j)th detector in the nth frame, i.e.,

$$e_n(i,j) = T_n(i,j) - (w_n(i,j) \cdot Y_n(i,j) + b_n(i,j)), \tag{10}$$

where

$$T_n(i,j) = \mathrm{FFT}^{-1}(\bar{\hat{X}}_{n-1}(u,v)e^{-2\pi j(ud_i+vd_j)}). \tag{11}$$

In particular, when the translation of two frames is of an integral pixel, then Eq. (11) can be transformed as

$$\begin{aligned} e_n(i,j) = {} & (w_n(i-d_i,j-d_j) \cdot Y_{n-1}(i-d_i,j-d_j) \\ & + b_n(i-d_i,j-d_j)) - (w_n(i,j) \cdot Y_n(i,j) + b_n(i,j)). \end{aligned} \tag{12}$$

To minimize the error $e_n(i,j)$ in the mean square error sense, a functional J is defined as

$$\begin{aligned} J(i,j) &= \sum_n e_n(i,j)^2 \\ &= \sum_n (T_n(i,j) - (w_n(i,j) \cdot Y_n(i,j) + b_n(i,j)))^2, \end{aligned} \tag{13}$$

where the correction parameters $w_n(i,j)$ and $b_n(i,j)$ must be recursively updated in order to minimize the cost function equation [Eq. (13)] that allows good NUC performance. Now, if we minimize Eq. (13) with respect to the parameters $w_n(i,j)$ and $b_n(i,j)$ using a stochastic gradient-descent strategy [9,17] over frames, the correcting parameters can be updated as

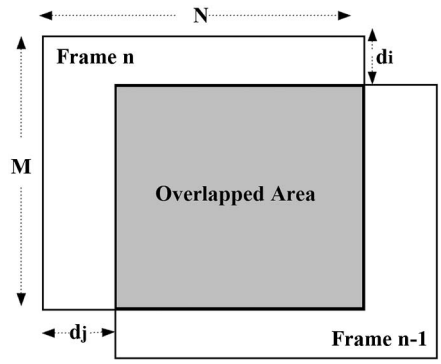

Fig. 1. Schematic diagram of the overlay of two frames.

where the parameter a is known as the learning rate. It should be pointed out that the correction parameters are only updated in the overlapped part between frame $n-1$ and frame n. The learning rate a stands for the step size of each iteration. The value of a governs the convergence behavior of the algorithm. A higher convergence speed will be gained with a larger a, while good stability of the algorithm can be achieved with a relatively small a. The block scheme of the whole algorithm is shown in Fig. 2, where a one-frame delay element is represented as a box with a z^{-1} symbol.

D. Convergence

In the previous subsection, the LMS algorithm with the error function of Eq. (9) is used to realize the iterative estimation of correction gain and offset parameters. But there is nothing to prove the rationality of the error function. Here, a simple analysis of when the relative displacement is of an integral number is undertaken. Then, the cost function J should be

$$\begin{aligned} J(i,j) &= \sum_n e_n(i,j)^2 \\ &= \sum_n ((w_n(i-d_i,j-d_j) \cdot Y_{n-1}(i-d_i,j-d_j) \\ &\quad + b_n(i-d_i,j-d_j)) - (w_n(i,j) \cdot Y_n(i,j) + b_n(i,j)))^2. \end{aligned} \tag{16}$$

Substitute Eq. (1) into Eq. (16):

$$\begin{aligned} J(i,j) = \sum_n (& (w_n(i-d_i,j-d_j) \cdot g_{n-1}(i-d_i,j-d_j) \\ & \cdot X_{n-1}(i-d_i,j-d_j) \\ & + w_n(i-d_i,j-d_j)o_{n-1}(i-d_i,j-d_j) \\ & + b_n(i-d_i,j-d_j)) \\ & - (w_n(i,j) \cdot g_n(i,j) \cdot X_n(i,j) + w_n(i,j) \cdot o_n(i,j) \\ & + b_n(i,j)))^2. \end{aligned} \tag{17}$$

If the registration error and change of irradiance of the scene can be ignored, $X_{n-1}(i-d_i,j-d_j)$ is the irradiance that the focal plane's (i,j)th detector in the nth frame has collected:

$$X_{n-1}(i-d_i,j-d_j) = X_n(i,j). \tag{18}$$

If Eq. (17) is required to be a minimum, it is clear that

$$\begin{aligned} & w_n(i-d_i,j-d_j) \cdot g_{n-1}(i-d_i,j-d_j) = w_n(i,j) \cdot g_n(i,j), \\ & w_n(i-d_i,j-d_j) \cdot o_{n-1}(i-d_i,j-d_j) + b_n(i-d_i,j-d_j) \\ & \quad = w_n(i,j) \cdot o_n(i,j) + b_n(i,j). \end{aligned} \tag{19}$$

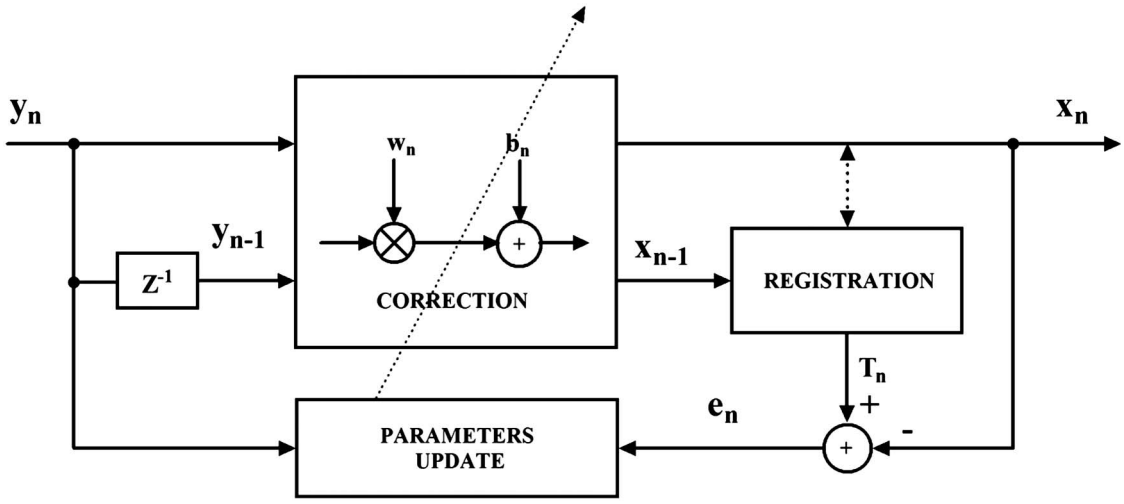

Fig. 2. Block diagram of the proposed algorithm.

It should be presumed that the motion between two adjacent frames is random, n is large enough, and the nonuniformity drifts very slowly in time and is almost fixed with respect to frame index n. Thus,

$$\begin{aligned} &w_n(i,j)\cdot g_n(i,j) = w_n(k,l)\cdot g_n(k,l),\\ &w_n(i,j)\cdot o_n(i,j) + b_n(i,j) = w_n(k,l)\cdot o_n(k,l) + b_n(k,l),\\ &\forall i,j,k,l \in \mathbf{Z}, \qquad i,l \le M, \qquad j,k \le N. \end{aligned} \tag{20}$$

Without loss of generality, we assume

$$\begin{aligned} &w_n(i,j)\cdot g_n(i,j) = 1,\\ &w_n(i,j)\cdot o_n(i,j) + b_n(i,j) = 0,\\ &\forall i,j \in \mathbf{Z}, \qquad i \le M, \qquad j \le N. \end{aligned} \tag{21}$$

Then we can get

$$w_n(i,j) = \frac{1}{g_n(i,j)}, \qquad b_n(i,j) = -\frac{o_n(i,j)}{g_n(i,j)}. \tag{22}$$

It can be seen from the above analysis that minimizing the cost function J is equivalent to approaching the ideal correction gain and offset. Hence, it is reasonable to set the corresponding value in frame $n-1$ as the "target value" of the (i,j)th detector in the nth frame. With the increase of iteration times, the error will gradually decrease, making any two detectors with the same scene generate the same output value. When J is minimized to zero, that means the nonuniformity of the IRFPA has been totally removed, then the LMS iteration has reached steady state. However, due to the drift of nonuniformity, registration error, local motion between images, and the temporal noise, the algorithm can never achieve steady state. Therefore, the algorithm should not stop iterating to guarantee the correction of the temporal drift of the FPN. Note that, if a significant number of bad pixels are present, a bad pixel detection and replacement method may be required prior to the registration to produce an unbiased "desired" image.

3. COMPARATIVE STUDY OF RELATED METHODS

In this section, the proposed IRLMS method is compared with two well-established NUC techniques. The first one is Scribner's algorithm [9], which is also called LMS for short since it is a LMS-based technique. It is a representative of statistical SBNUC methods and has been widely studied because of its small computational load and memory requirement. Besides, both IRLMS and the Scribner's algorithm use the stochastic steepest decent technique to optimize the correction coefficients. The second one is MCA [14], because it is a representative of registration-based SBNUC methods and shares the similar idea that each detector should have an identical response when observing the same scene point for a short time. The comparisons are focused on the rationality and computational load in this section. The comparisons of their experimental performance will be illustrated in Section 5.

A. Rationality and Feasibility

The basic idea of Scribner's method is that applying a local neighborhood interpolating function to create the "desired" image then using the LMS algorithm based on the stochastic gradient drives the corrected image toward it. This method works very well when the fixed pattern noise shows less spatial correlation since the interpolating function is usually a spatial low-pass smoothing filter and the FPN can be effectively averaged. However, it is clear that the local spatial average is not always a good estimate for the real incident infrared irradiance. Thus, an enhanced version of the Sicribner's method, known as gated adaptive LMS (GALMS) [17] was recently proposed to counteract the ghosting artifacts caused by this inconsistency. In the GALMS method, the updating process halts to prevent the signal of the scene being assumed as the nonuniformity noise when the global motion is insufficient. In addition, an adaptive learning rate is introduced to increase the efficiency of the learning process. The GALMS method largely solves the "burn-in" problem in Scribner's method and shows great improvement in NUC performance.

In contrast, the MCA technique developed by Hardie *et al.* [14] employs the idea that the average of properly registered observed image frames gives an unbiased estimate of the true scene. For offset-only correction, i.e., the gain is assumed

uniform across all detectors with a value of unity, the offset parameters are given by simply subtracting the observed image from the true scene estimate. For the linear model [Eq. (1)], gain and offset parameters can be obtained by using a least-square fit. MCA can get great NUC results within only tens of frames and introduce fewer artifacts than the GALMS since the estimate of true scene is more accurate and reasonable. Compared with GALMS, the MCA technique does not use any statistical assumptions about the scene and each point of the true scene is determined by the pixel values that represent the same scene position. Thus, the true signal is enhanced while the fixed pattern noise is reduced, and the interference of true scene signals in the correction parameters is almost eliminated through the registration operation, while each point of the "desired" image of GALMS is only a coarse approximation from its neighborhood. And, inevitably, the correction image will suffer degradation in visual quality to varying degrees.

As we know, in the MCA method, the most critical step is creating the true scene estimate, i.e., a panoramic image. With the estimate of the desired scene data in hand, subsequent NUC can be performed straightforwardly. However, it is usually impractical to generate a panoramic image first and then correct the IRFPA. So, in general conditions, panorama accumulation and NUC should be performed simultaneously. However, there is little information available in the literature [14] about these problems, such as how to update the panorama, especially when the scene does not remain sufficiently unchanged over time, or how to perform the algorithm in a more efficient way for practical applications.

Compared with GALMS and MCA, the "desired" image in IRLMS is less intuitive since it is only a properly shifted frame without any denoising operation, such as spatial smoothing or temporal averaging. In IRLMS, we do not explicitly drive the corrected image toward the true scene value, however; we focus only on the actual task for NUC, i.e., making any two detectors with the same scene produce the same output value. As discussed in Subsection 2.C, it could get an equivalent NUC effect while avoiding the strenuous work of estimating the true scene. When solved by the stochastic gradient-descent method, the update is a function of only the current frame and the previous frame, which makes the algorithm very easy to implement in practice.

There are grounds for believing that the IRLMS method produces even fewer artifacts and has higher steady-state accuracy. First, we assume that the observed scenes do not change significantly during the time between two consecutive frames. This is often reasonable for most cases because of the rather short time. Then, the IRLMS method automatically has no update when no motion is present, which is optimum with regards to "burn-in" since SBNUC generally requires motion between frames. Finally, the updating process almost stops when the nonuniformity is totally removed since the properly shifted two adjacent image frames are almost the same, which prevents the correction coefficients from being wrongly updated.

B. Computational Complexity and Storage Demands

Small computational load and low memory requirements are two important aspects for real-time applications. It seems that GALMS is most suitable for real-time performance because there is no need for registration. However, it poses more problems for real-time implementations, especially if a large filter mask is required while an IRFPA's nonuniformity mostly concentrates on low spatial frequency and shows great spatial correlations. Obviously, the calculation of GALMS is mainly concentrated on spatial smoothing and calculating local variance for each pixel. Usually, the local variance can be calculated within a smaller window and the spatial smoothing convolution can be accelerated by separating the two-dimensional filter into two one-dimensional filters. So the computational complexity of GALMS in this case is $O(2n_wMN)$ for a $n_w \times n_w$ filter window.

MCA involves many calculations since it is not an iterative algorithm. Without consideration of the registration operation, the complexity of the correction operation is $O(LMN)$ for offset-only correction and $O(8LMN)$ for linear correction because the least-square fitting involves some matrix operations [14]. L stands for the number of frames used for estimation and usually L should be larger than 20 to ensure accuracy. In addition, the MCA methods require much more memory since a panoramic image must be stored.

However, for the IRLMS method, only three multiplications and two additions are required per sensor per update. Therefore, the complexity of the IRLMS algorithm is essentially determined by the registration method. The complexity of the registration algorithm can be reduced to $O(\kappa^{\frac{1}{2}}MN)$ without sacrificing accuracy [22]. There is no critical difference between a smaller κ and a larger κ since the actual registration accuracy is largely determined by the level of nonuniformity. Further discussions concerning the registration accuracy under conditions of nonuniformity are presented in Subsection 4.A. In general, $\kappa = 10$ is sufficient to meet the accuracy requirements since our method is an iterative algorithm. Therefore, the computational complexity of IRLMS is even lower than that of the GALMS algorithm with a large window. In addition, IRLMS can be implemented with very little memory since the extra storage demand is only one previous image frame.

4. KEY PERFORMANCE ISSUES

In this section, the performance of the proposed correction algorithm is studied using images and sequences corrupted by simulated nonuniformity. Three main areas are studied: the accuracy of registration in the presence of fixed pattern noise, choosing a proper learning rate, and displacement between frames.

A. Registration Accuracy with Nonuniformity

The performance of NUC algorithm proposed in this paper depends greatly on the accuracy of estimation of the global motion between the frames. In order to estimate the accuracy of the registration algorithm adopted by this paper under the conditions of fixed pattern noise, an 8 bit gray-scale 320×256 image pair with known relative displacement is studied. Normal distributed gain and offset nonuniformity are applied to the image pair to study the relationship between registration error and level of nonuniformity. Figure 3 shows the relationship between the mean absolute error (MAE) of translation estimates with the levels of gain and offset.

Under an ideal circumstance, the registration MAE should be controlled under 0.1. But the proposed algorithm only takes the relative displacement between two frames into consideration and the error does not accumulate with the

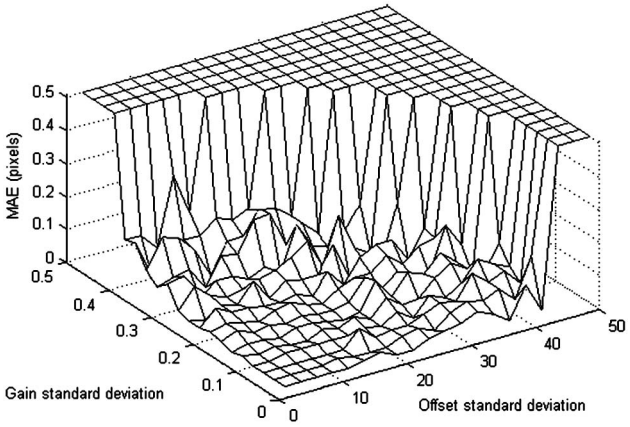

Fig. 3. Mean absolute error of translation estimates for various levels of gain and offset nonuniformity in an 8 bit gray-scale image.

frames. Therefore, a value under 0.3 can be accepted, that is, the standard deviations of gain and offset are, respectively, under 0.4 and 40. Besides, nonuniformity will decrease with the frame number and the registration accuracy will increase gradually. If the level of the IRFPA's nonuniformity exceeds this range, the noise becomes too dominant in the image and no relative translation can be detected. At this point, calibration-based NUC methods or statistical scene-based algorithms can be performed beforehand since they require no registration. Once the nonuniformity is reduced to some degree, the proposed method can be used for periodic updates.

B. Learning Rate Analysis

The following experiment is designed for studying the proposed IRLMS method under different learning rates. The infrared sequence with artificial nonuniformity is generated from a clear 300 frame infrared video sequence acquired at 50 frames per second (FPS), using a synthetic gain with a unit-mean Gaussian distribution with standard deviation of 0.2, and a synthetic offset with a zero-mean Gaussian distribution with standard deviation of 40. The experiment is repeated for three learning rate values: 0.025, 0.05, and 0.1. The metric used to measure the NUC performance is given by the root-mean-square error (RMSE), which is defined as

$$\mathrm{RMSE} = \sqrt{\frac{1}{M \cdot N} \sum_{i,j} (X(i,j) - \hat{X}(i,j))^2}, \tag{23}$$

where $X(i,j)$ is the (i,j)th pixel's value of the true frame, while $\hat{X}(i,j)$ is the pixel's value of the corrected frame. RMSE is used to measure the overall difference between a clean reference image against its noisy and nonuniformity corrected versions. The RMSE curves versus frame numbers of three different learning rates are shown in Fig. 4.

It can be observed from Fig. 4 that smaller learning rates lead to slower and softer performance curves, but they are more stable than those of larger values. Using $a = 0.1$, RMSE can be reduced below 20 within only 20 frames, after which relatively large fluctuations appear in the curve; especially when it is near the 100th frame, RMSE rebounds to the position of nearly 30, and then the curve fluctuates around 20. When a is set as 0.025, the curve falls rather stably and, after 300 frames, the RMSE reaches 5.39. However, the convergence speed is relatively slow and the RMSE does not fall below 20 until 100 frames are used. Therefore, a good balance among correction quality, convergence speed, and stability must be considered. Considering these, relatively ideal convergence speed and stability can be attained when a is 0.05.

C. Relative Translation Analysis

During the previous analysis, we found that using $a = 0.05$ provides a reasonable trade-off between convergence speed and stability. Apart from learning rate, the displacement between frames also affects the performance of the proposed algorithm. For some high-frame-rate infrared cameras, whose frame rates can exceed 200 FPS, almost no translation between two frames can be detected in most cases. The performance of the proposed method will obviously degenerate if we still use two adjacent frames to register. A simple idea in this case is to perform correction by choosing frame pairs with intervals of k rather than 1. Then, the error function Eq. (9) can be modified as

$$e_n(i,j) = \hat{X}_{n-k}(i - d_i, j - d_j) - \hat{X}_n(i,j). \tag{24}$$

By adjusting the value of k, the relative translation of the image pair can be controlled.

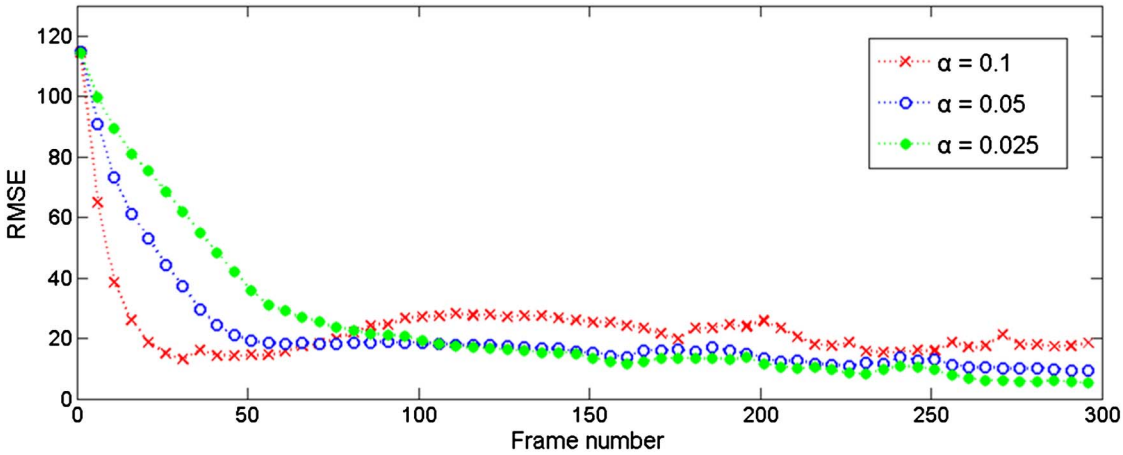

Fig. 4. (Color online) RMSE versus frame number using different learning rates.

The displacement between two adjacent frames is the primary focus of this test. In order to test the relationship between displacement between two adjacent frames and the efficiency of correction, a 50 FPS 320×256 long-wave infrared camera is used. However, it moves very slowly; thus, a 300 frame "high-frame-rate" video sequence is gained. Then the sequence is corrupted with the same level of nonuniformity as in Subsection 4.B. The average displacement d is defined as

$$d = \frac{\sum_{n=1}^{m} \sqrt{d_i(n)^2 + d_j(n)^2}}{m}, \tag{25}$$

where m is the number of iteration times, and $d_i(n)$ and $d_j(n)$ are, respectively, the horizontal and vertical shifts between the mth image pair. Different values of k are chosen to generate different values of d. With different values of d, the final RMSE values after 300 iterations are compared. The relationship between RMSE and d is shown in Fig. 5.

From Fig. 5, it is found that the final RMSE is relatively large when the average relative displacement d is either too large or too small. If the value of d is too small, the pixel will be in less touch with the pixels relatively far from it, so it will be hard for the nonuniformity of low spatial frequency to get adequate correction. If the value of d is too large, the overlapped area between two frames will be too small, resulting in fewer updated correction parameters in each iteration. Meanwhile, the registration error will increase with d since the images obviously share less and less of the scene data. Fortunately, d should be controlled within the range of 2–8, ideally, which is not that narrow. When setting the value of k, it is best that the value of d falls into this range. However, there is no guarantee that the value of k is appropriate throughout the video sequence and it cannot be properly chosen beforehand in many practical applications. A more practicable solution is to update the correction coefficients only if sufficient displacement is measured between the current frame and a reference frame. The reference frame is only refreshed when the correction coefficient is updated. Figure 5 can be used as the reference for choosing this trigger displacement.

5. EXPERIMENTAL RESULTS

To compare the various SBNUC algorithms, and, in particular, to demonstrate the efficacy of the proposed IRLMS algorithm, we apply our method to both simulated and real data.

A. Applications to Simulated Nonuniformity

The performance of IRLMS is studied and compared with the performance of GALMS and MCA by applying these algorithms to 14 bit infrared image sequences corrupted by simulated nonuniformity. The infrared sequences with artificial nonuniformity are generated from a clear 600 frame infrared video sequence with the same level nonuniformity as in Subsection 3.B. The metric used to measure the NUC performance is given by the peak signal-to-noise ratio (PSNR), which is widely used to quantify the differences between two images, and it is defined as

$$\mathrm{PSNR} = 20 \log_{10}\left(\frac{2^b - 1}{\mathrm{RMSE}}\right), \tag{26}$$

where b represents the number of bits per pixel in the image, which, in this case, is equal to 14. The PSNR of the corrupted image sequences with simulated nonuniformity are about 23.5 dB for all the frames. Larger values for the PSNR indicate better performance.

The GALMS method is tested with a step size of 0.05 and two window sizes of 3×3 for an average filter and 21×21 for a Gaussian low-pass filter (recommended in [17]). The change threshold is set to 20. The learning rate a takes the value of 0.05 in IRLMS, and update trigger displacement is set to 3.5. The single-step discrete Fourier transform approach [22] is adopted for the implementation of the registration method. In MCA, the first 30 frames are registered and a panoramic image is created before correction. Then the correction gain and offset are estimated using the 30 frames by least-square fitting and the following frames are corrected using the estimated parameters.

1. Nonuniformity Correction Performance

The PSNR evolution of the three tested algorithms is displayed in Fig. 6. The curve of MCA does not increase before frame 30 since its correction parameters are calculated by the first 30 frames. It can be noted from Fig. 6 that the IRLMS method significantly outperforms the other methods due to its faster convergence speed and higher PSNR. For the first 50 frames, the curves of IRLMS and GALMS have a stable increasing tendency. The speed of the IRLMS algorithm takes the lead and it only takes 50 frames to cross the 35 dB barrier. For the rest of the sequence, it never goes below this quality. GALMS with a 3×3 window converges slower than IRLMS for the first 150

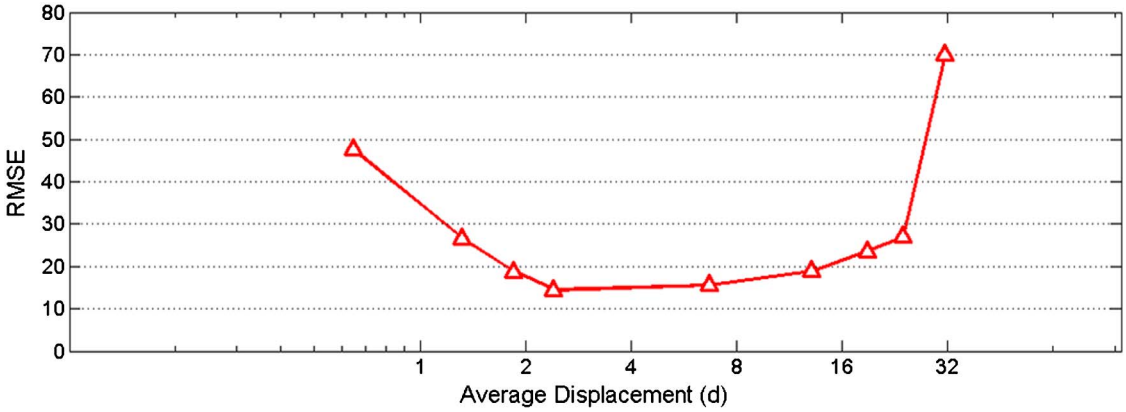

Fig. 5. (Color online) Relationship between RMSE and average displacement d (after 300 times iteration, learning rate $a = 0.05$).

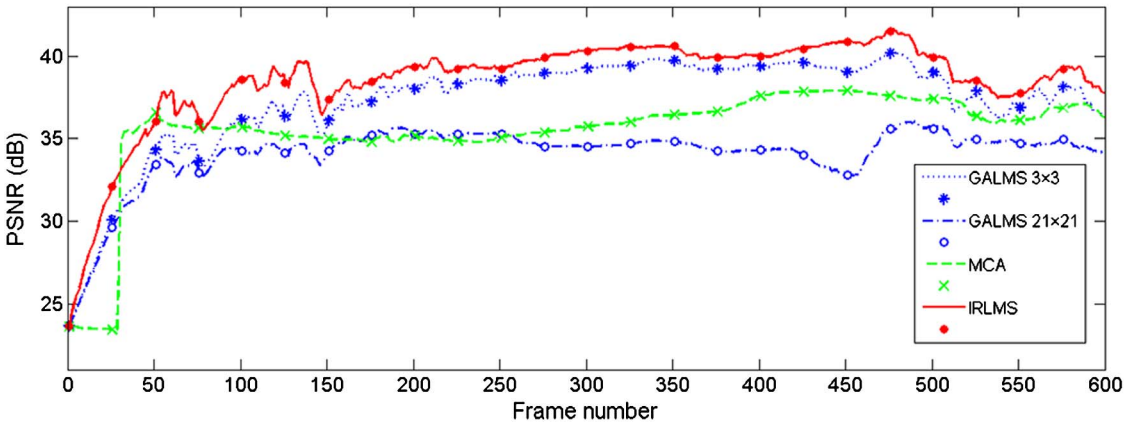

Fig. 6. (Color online) PSNR results of the synthetic noisy test sequence corrected using different NUC methods.

frames and it keeps a gap of nearly 1.2 dB below IRLMS for the remaining test videos. The performance of GALMS with a 21×21 window is worse than that achieved with a smaller window. This is mostly due to the spatial independence of the nonuniformity. A 3×3 window is large enough for averaging the nonuniformity with a Gaussian distribution, while a larger window leads to greater estimation errors. Using the parameters calculated by the first 30 frames, the PSNR of MCA for all subsequent frames is around 36 dB. It is rather high in the early stage, but it is overtaken by IRLMS and GALMS with a 3×3 window subsequently, since its correction parameters are not updated.

Figure 7 (Media 1) shows the images for the 570th frame. Figure 7(a) shows the raw image corrupted with simulated nonuniformity. The outputs using GALMS, MCA, and IRLMS are shown in Figs. 7(b)–7(e), respectively. In the outputs of GALMS, some ghosting artifacts of the wire poles can be appreciated. There is also some residual nonuniformity that can be perceived in the output of MCA. However, we can hardly see any ghosting artifact in the IRLMS's output and the level of residual nonuniformity is rather low. In order to render the results more perceptible, the error images for these methods are shown in Fig. 8, scaled identically. It is clear that the error images of GALMS have more scene information. These results are ratified by the PSNR of each image displayed.

2. Computational Efficiency

In Subsection 3.B, we developed a brief analysis on the computational complexity and memory demand of the three algorithms. In real computer systems, however, memory

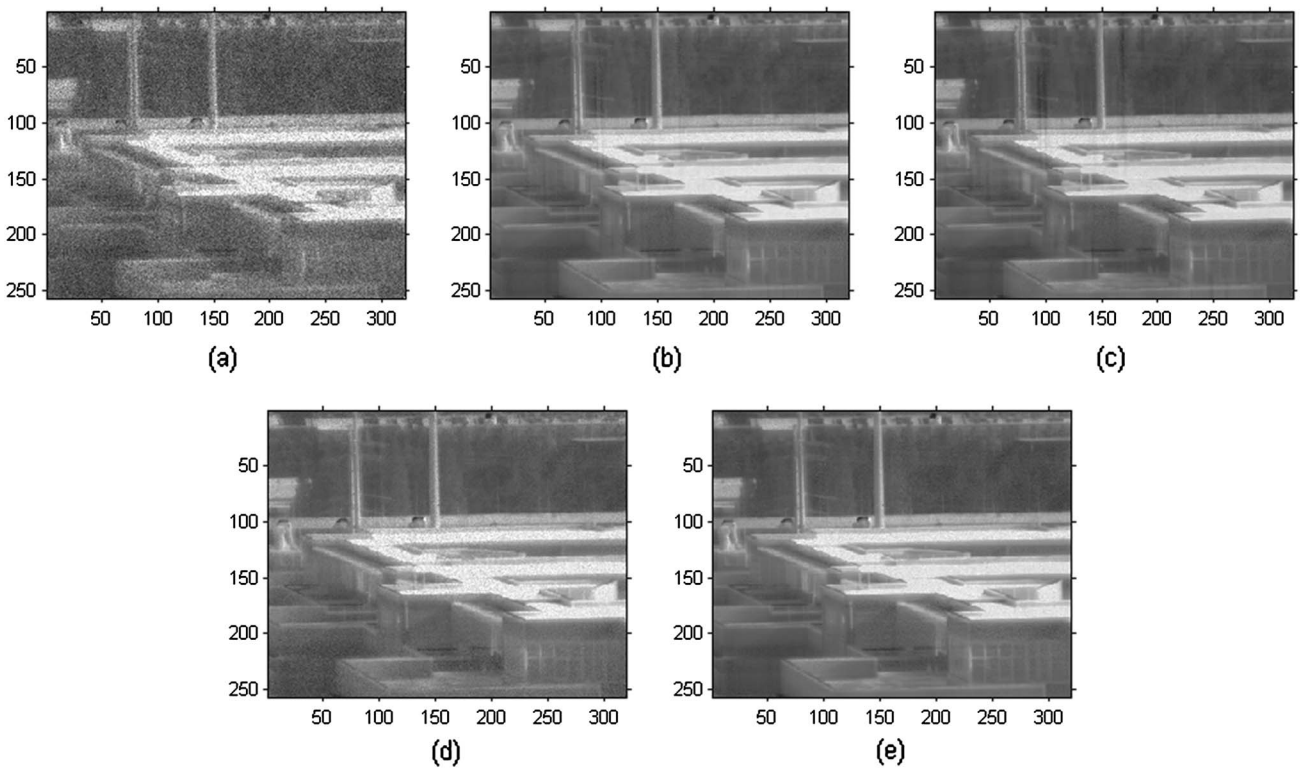

Fig. 7. (Media 1) Simulated nonuniformity image results. (a) Image with simulated gain and offset nonuniformity (PSNR = 23.6 dB). (b) Corrected with GALMS 3×3 (PSNR = 36.6 dB). (c) Corrected with GALMS 21×21 (PSNR = 34.7 dB). (d) Corrected with MCA (PSNR = 36.4 dB). (e) Corrected with IRLMS (PSNR = 38.3 dB).

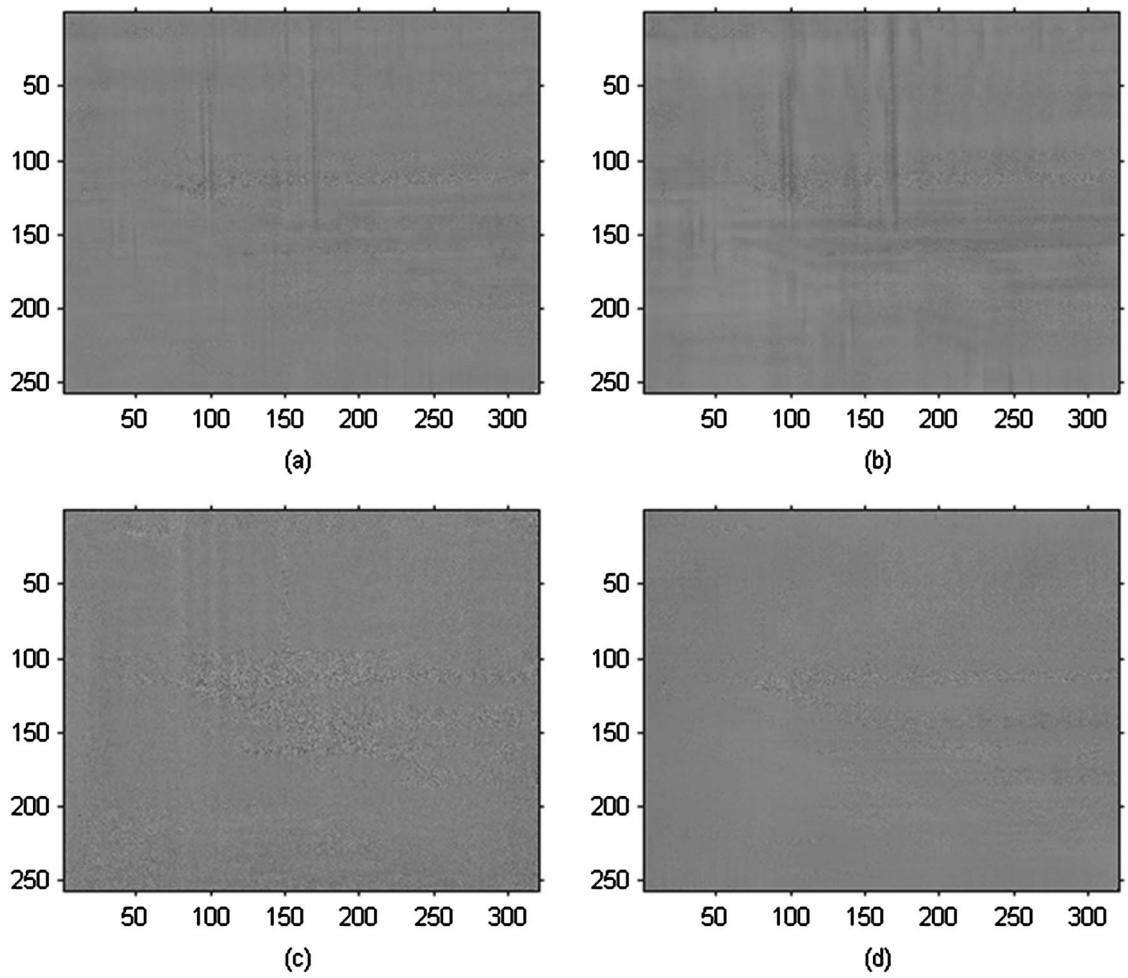

Fig. 8. Error images for (a) GALMS 3×3; (b) GALMS 21×21; (c) MCA; (d) IRLMS. All images are scaled to the same display range.

hierarchy, operating system planning, and many other practical factors must be taken into account and a theoretical analysis is not enough. We are more interested in how fast the different methods are in actual operation. These tests were made with an Intel Core2 Duo T5870 2.0 GHz processor and 2 Gbyte RAM in conjunction with MATLAB's cputime function. In MCA, the estimation of the linear correction parameters takes approximately 55 s. So here we only compare IRLMS with GALMS. Table 1 shows a rough average of CPU time consumed per frame of the two algorithms. It seems that IRLMS is more time consuming than GALMS with a 3×3 average window and its speed is very close to that of GALMS with a 21×21 Gaussian window. This is probably because most of the functions GALMS used are provided by MATLAB, while the registration function used in IRLMS is a self-edit and without any significant optimization.

Table 1. Average CPU Time Consumed per Frame for GALMS and IRLMS

	GALMS 3×3	GALMS 21×21	IRLMS
Average CPU time per frame (s)	0.069	0.172	0.181

B. Applications to Real Infrared Data

In this subsection, the algorithm put forward is applied to two sets of real infrared data. The first set of data was collected at 11 a.m. by using a 320×256 HgCdTe FPA camera operating in the 3–5 μm range and working at 25 FPS. The second set was acquired at 6 p.m. by using another 320×256 HgCdTe FPA camera operating in the 8–14 μm range and at a rate of 50 FPS. Two sample images of the two test sequences are shown in Fig. 9. A serious striping effect can be found in Fig. 9(a) and it mainly exists in the high spatial frequency of the image, while the FPN in Fig. 9(b) shows more low spatial frequency characteristics.

When dealing with real infrared images, it is not always possible to obtain the calibration data needed to perform a radiometrically accurate correction to be used as a reference for comparison purposes, so the PSNR cannot be calculated. However, the roughness index ρ is often used as a measure or indicator of the amount of FPN present in a real image. The index is calculated as follows:

$$\rho=\frac{\|h_1*I\|_1+\|h_2*I\|_1}{\|I\|_1}, \tag{27}$$

where h_1 and h_2 are a horizontal and a vertical difference filter, respectively, I is the image under analysis, $\|I\|_1$ is the L_1 norm of I, and $*$ represents discrete convolution. Note

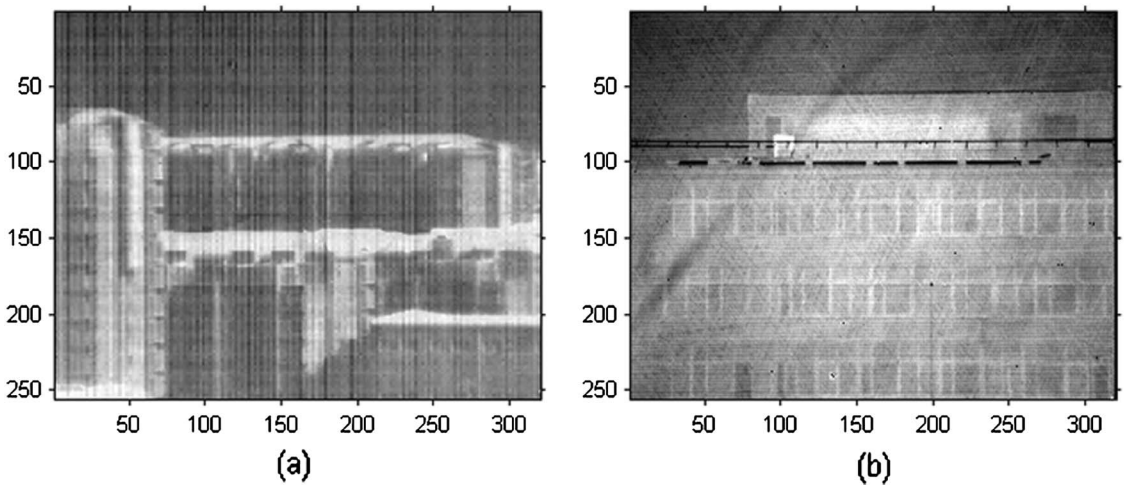

Fig. 9. Sample images of the two test sequences. (a) Frame 1 of the first test sequence. (b) Frame 1 of the second test sequence.

the roughness index ρ does not require the knowledge of the true image, so it can be used as a measure of NUC in real infrared data. In addition, the video sequences were generated from all the different versions of corrected data for visual analysis. Afterward, the NUC over the two test sequences was done using the selected algorithms with the same parameter sets as in Subsection 5.A. The results of the mean roughness over each sequence are presented in Table 2. From there, the IRLMS clearly outperformed all the other algorithms in the mean sense.

Table 2. Mean Roughness $\rho(\times 10^{-3})$ Results for the Two Test Sequences

Algorithm	Sequence I	Sequence II
Unprocessed	1.974	1.292
GALMS 3×3	1.313	0.761
GALMS 21×21	1.219	0.662
MCA	1.201	0.691
IRLMS	1.141	0.613

A performance measurement like the roughness index can help, but it does not necessarily indicate good correction performance or whether there is the presence of artifacts. Therefore, the video sequences must be watched to perform a visual evaluation (Media 2 and Media 3). From the two video sequences, it is very noticeable that the IRLMS compensates the nonuniformity the fastest and performs the best over the

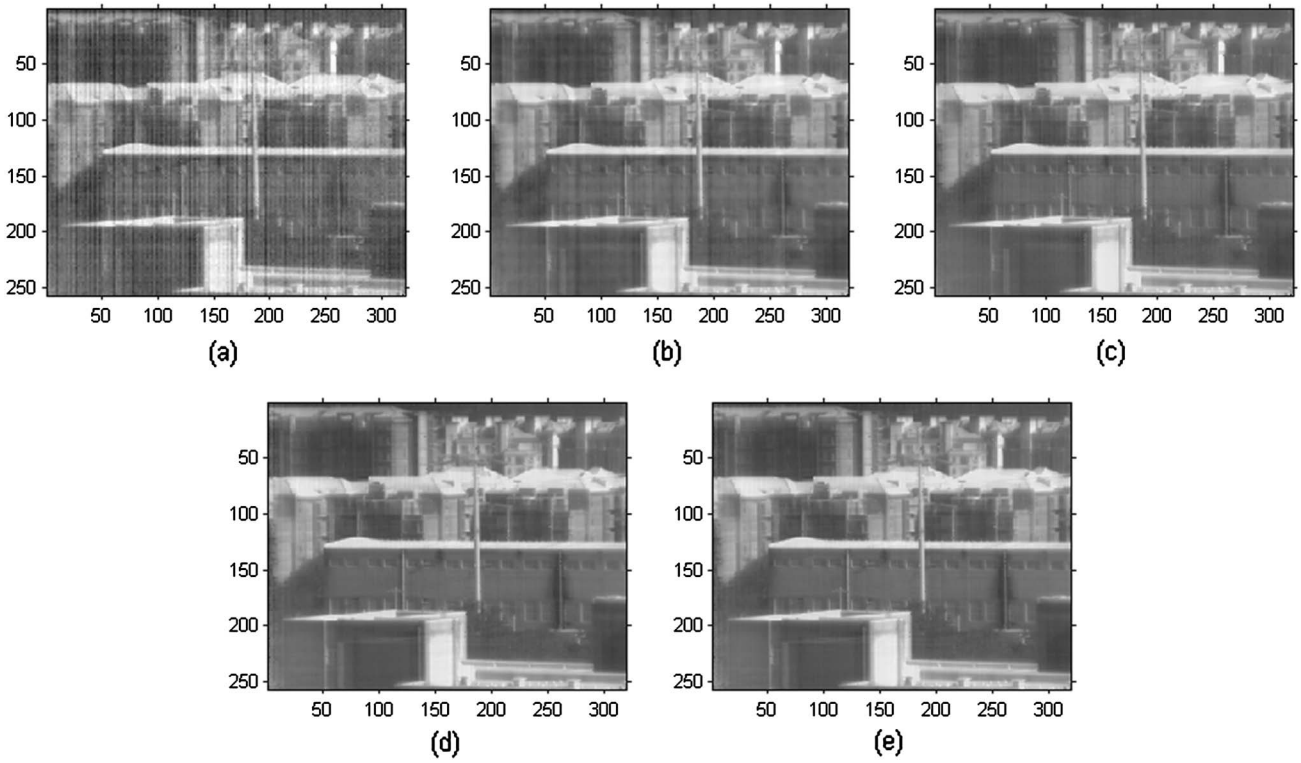

Fig. 10. (Media 2) NUC performance comparison of frame 50 of the first test sequence. (a) Unprocessed ($\rho = 2.059 \times 10^{-3}$); (b) GALMS 3×3 ($\rho = 1.552 \times 10^{-3}$); (c) GALMS 21×21 ($\rho = 1.419 \times 10^{-3}$); (d) MCA ($\rho = 1.371 \times 10^{-3}$); (e) IRLMS ($\rho = 1.355 \times 10^{-3}$).

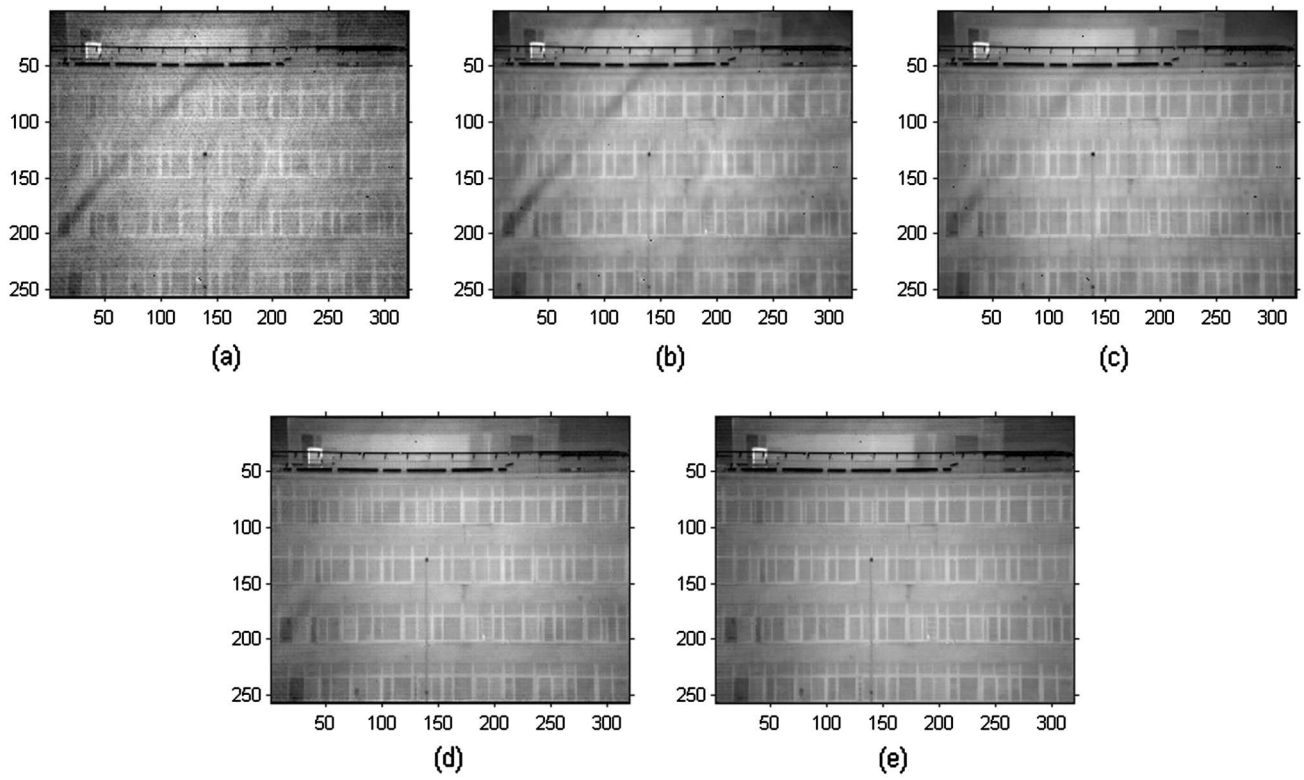

Fig. 11. (Media 3) NUC performance comparison of frame 50 of the second test sequence. (a) Unprocessed ($\rho = 1.632 \times 10^{-3}$); (b) GALMS 3×3 ($\rho = 1.251 \times 10^{-3}$); (c) GALMS 21×21 ($\rho = 1.129 \times 10^{-3}$); (d) MCA ($\rho = 0.971 \times 10^{-3}$); (e) IRLMS ($\rho = 0.852 \times 10^{-3}$).

two sequences. Besides, it effectively generates much fewer ghosting artifacts than the other techniques. Frame samples of the two sequences at different stages of the NUC process are presented in Figs. 10–13.

Figures 10 and 11 show frame 50 of each individual subsequence. It can be seen that the proposed IRLMS algorithm almost eliminated the FPN within only 50 frames. It is no wonder that MCA also gives good results because its correction

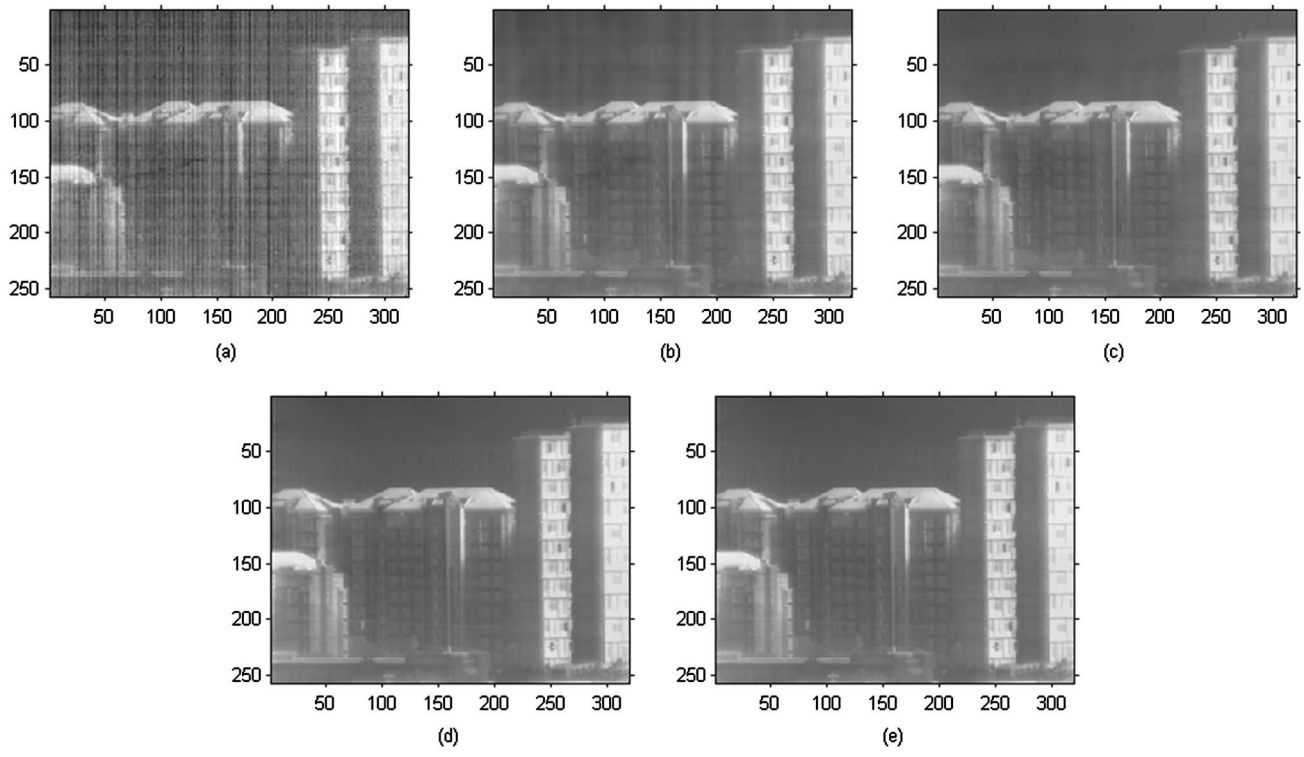

Fig. 12. (Media 2) NUC performance comparison of frame 150 of the first test sequence. (a) Unprocessed ($\rho = 1.769 \times 10^{-3}$); (b) GALMS 3×3 ($\rho = 0.997 \times 10^{-3}$); (c) GALMS 21×21 ($\rho = 0.929 \times 10^{-3}$); (d) MCA ($\rho = 0.871 \times 10^{-3}$); (e) IRLMS ($\rho = 0.855 \times 10^{-3}$).

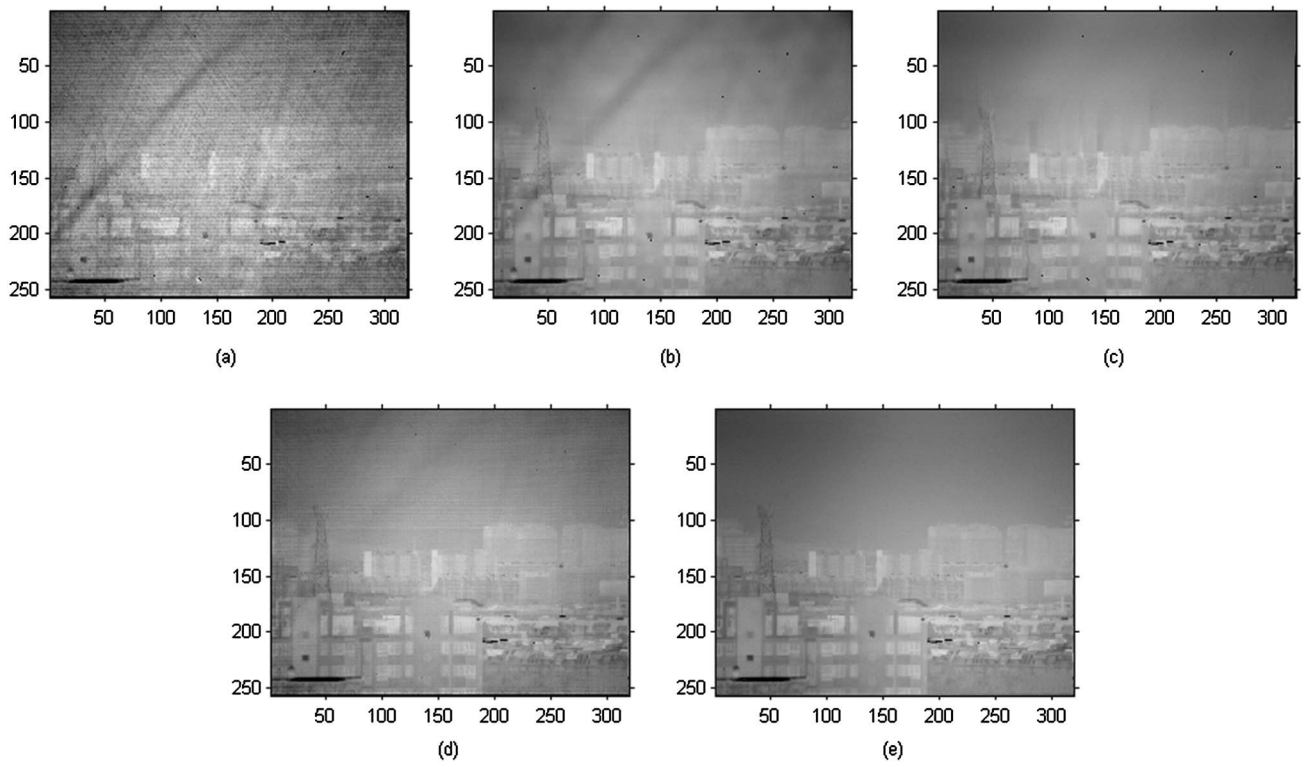

Fig. 13. (Media 3) NUC performance comparison of frame 230 of the second test sequence. (a) Unprocessed ($\rho = 1.629 \times 10^{-3}$); (b) GALMS 3×3 ($\rho = 0.677 \times 10^{-3}$); (c) GALMS 21×21 ($\rho = 0.609 \times 10^{-3}$); (d) MCA ($\rho = 0.681 \times 10^{-3}$); (e) IRLMS ($\rho = 0.543 \times 10^{-3}$).

parameters are calculated by thoroughly examining the first 30 frames. The GALMS method, in contrast, converges more slowly. Because of the spatial correlations of the nonuniformity, a 3×3 average window is probably too small to smooth the nonuniformity effectively, leading to a much slower convergence rate than the Gaussian cases discussed in Subsection 5.A. GALMS with a 21×21 window obtains better results compared with the one with a 3×3 window. But in its outputs, especially in Fig. 11(b), some low spatial frequency nonuniformity and ghost artifacts are clearly visible.

Figures 12 and 13 show frame 150 of the first sequence and frame 230 of the second sequence, respectively. It can be seen that the nonuniformity presented in the raw frame has been notably reduced by all the NUC methods. However, the ghosting artifacts can be perceived in the outputs of GALMS. Also, the residual low spatial nonuniformity is also visible in the output of the GALMS with a 3×3 window. In the outputs of MCA, we can see some residual nonuniformity, especially near the borders of the images, because the parameters are estimated using only 30 frames and all these frames may not share the exact same field of view. However, in the correction outputs of IRLMS, the residual nonuniformity is too low to be detected by the naked eyes, and almost no ghosting artifact can be detected.

6. DISCUSSION AND CONCLUSIONS

In this paper, a novel interframe-registration-based correction for NUC in IRFPAs has been presented. This method uses a phase-correlation method to estimate the motion between two adjacent images and an LMS algorithm to calculate the gain and offset correction coefficient of the FPA. The mean square error between the two registered images is minimized to make every two detectors with the same scene produce the same output value. Thus, the accumulation of the registration error can be avoided and the NUC is easily obtained. The strength of the proposed algorithm lies in its reasonably simple assumptions and smaller calculation and memory requirements, which make it more competitive in real-time processing.

Some experiments have been done to test the proposed algorithm. It is shown that its performance can be further improved by properly controlling the update process. In addition, we have compared our method with the GALMS and MCA SBNUC algorithms, which represent perhaps the most commonly employed statistical method and registration-based method. Experimental results demonstrate its great performance and capabilities to avoid undesirable effects.

Since our method is based on registration, it also shares some limitations with most registration-based NUC methods and may not work for some particular conditions. The correction errors may result from local motion, scene rotation, changes of scene irradiation, etc. When the scene objects are imaged at a relatively small distance, warping of the images should also be taken into account. However, corresponding countermeasures are not so complicated in our method. A possible solution is to create the reference frame using a more complex registration method that takes these factors into consideration.

REFERENCES

1. D. A. Scribner, M. Kruer, and J. Killiany, "Infrared focal plane array technology," Proc. IEEE **79**, 66–85 (1991).
2. D. Scribner, K. Sarkady, J. Caulfield, M. Kruer, G. Katz, and C. Gridley, "Non-uniformity correction for staring focal plane arrays using scene-based techniques," Proc. SPIE **1308**, 224–233 (1990).

3. A. Friedenberg and I. Goldbatt, "Nonuniformity two-point linear correction errors in infrared focal plane arrays," Opt. Eng. **37**, 1251–1253 (1998).
4. E. Gurevich and A. Fein, "Maintaining uniformity of IR focal plane arrays by updating offset correction coefficients," Proc. SPIE **4820**, 809–820 (2003).
5. M. Schulz and L. Caldwell, "Nonuniformity correction and correctability of infrared focal plane arrays," Infrared Phys. Technol. **36**, 763–777 (1995).
6. O. Riou, S. Berrebi, and P. Bremond, "Nonuniformity correction and thermal drift compensation of thermal infrared camera," Proc. SPIE **5405**, 294–302 (2004).
7. D. Scribner, K. Sarkady, M. Kruer, J. Caldfield, J. Hunt, M. Colbert, and M. Descour, "Adaptive retina-like preprocessing for imaging detector arrays," in *Proceedings of the IEEE International Conference on Neural Networks* (Institute of Electrical and Electronics Engineers, 1993), pp. 1955–1960.
8. J. G. Harris and Y. M. Chiang, "Nonuniformity correction using constant-statistics constraint: analog and digital implementations," Proc. SPIE **3061**, 895–905 (1997).
9. D. Scribner, K. Sarkady, M. Kruer, J. Caldfield, J. Hunt, M. Colbert, and M. Descour, "Adaptive nonuniformity correction for IR focal plane arrays using neural networks," Proc. SPIE **1541**, 100–109 (1991).
10. S. N. Torres, R. A. Reeves, and M. M. Hayat, "Scene-based nonuniformity correction method using constant-range: performance and analysis," in *Proceedings of 6th World Multiconference on Systemics, Cybernetics and Informatics* (2002), pp. 224–229
11. S. N. Torres and M. M. Hayat, "Kalman filtering for adaptive nonuniformity correction in infrared focal plane arrays," J. Opt. Soc. Am. A **20**, 470–480 (2003).
12. S. N. Torres, J. E. Pezoa, and M. M. Hayat, "Scene-based nonuniformity correction for focal plane arrays by the method of the inverse covariance form," Appl. Opt. **42**, 5872–5881 (2003).
13. W. F. O'Neil, "Dithered scan detector compensation," in *Proceedings of the 1993 International Meeting of the Infrared Information Symposium Specialty Group on Passive Sensors* (Infrared Information Analysis Center, 1993).
14. R. C. Hardie, M. M. Hayat, E. E. Armstrong, and B. Yasuda, "Scene-based nonuniformity correction using video sequences and registration," Appl. Opt. **39**, 1241–1250 (2000).
15. B. M. Ratliff, M. M. Hayat, and R. C. Hardie, "An algebraic algorithm for nonuniformity correction in focal-plane arrays," J. Opt. Soc. Am. A **19**, 1737–1747 (2002).
16. C. Zuo, Q. Chen, G. Gu, and W. Qian, "New temporal high-pass filter nonuniformity correction based on bilateral filter," Opt. Rev. **18**, 197–202 (2011).
17. R. Hardie, F. Baxley, B. Brys, and P. Hytla, "Scene-based nonuniformity correction with reduced ghosting using a gated LMS algorithm," Opt. Express **17**, 14918–14933 (2009).
18. J. Harris and Y. Chiang, "Minimizing the 'ghosting' artifact in scene-based nonuniformity correction," Proc. SPIE **3377**, 106–113 (1998).
19. D. L. Perry and E. L. Dereniak, "Linear theory of nonuniformity correction in infrared staring sensors," Opt. Eng. **32**, 1854–1859 (1993).
20. C. D. Kuglin and D. C. Hines, "The phase correlation image alignment method," in *Proceedings of the International Conference of the Cybernetics Society* (1975), pp. 163–165.
21. B. Marcel, M. Briot, and R. Murrieta, "Calcul de translation et rotation par la transformation de Fourier," Traitement du Signal **14**, 135–149 (1997).
22. M. Guizar-Sicairos, S. T. Thurman, and J. R. Fienup, "Efficient subpixel image registration algorithms," Opt. Lett. **33**, 156–158 (2008).